CHEMICAL REVIEWS

Review

pubs.acs.org/CR

Toward Cold Chemistry with Magnetically Decelerated Supersonic Beams

Edvardas Narevicius*,† and Mark G. Raizen‡

†Department of Chemical Physics, Weizmann Institute of Science, Rehovot 76100, Israel

‡Center for Nonlinear Dynamics and Department of Physics, The University of Texas at Austin, Austin, Texas 78712, United States

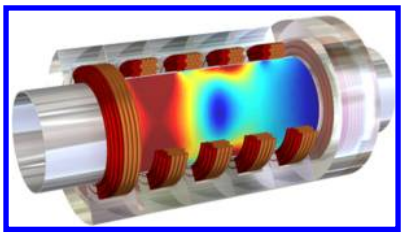

CONTENTS

1. INTRODUCTION

Cold chemistry[1,2] is an emerging field with many theoretical predictions and very few experiments.[3−5] Traditionally, cold chemistry has been pursued by the chemical physics and astrophysics communities. The primary focus so far has been on chemical processes at temperatures of 10−100 K, relevant to fundamental questions of composition and routes to complex molecule formation in the dense interstellar clouds or atmospheres of exoplanets.[6,7] Lower temperatures of ∼1 K and below bring us to a new regime where the de Broglie wavelength reaches the characteristic dimensions of the interaction potential and quantum effects become dominant. Indeed, even the dynamics of the most studied benchmark reaction of F + H_2 are shrouded in uncertainty at low temperatures! At higher temperatures there is almost a perfect agreement between theoretical predictions/calculations and experimental results.[8−10] In striking contrast, at low temperatures, the theoretical predictions of the reaction rate differ by orders of magnitude depending on a model or potential energy surface used in the calculation.[8] This is a manifestation of one of the "trademarks" of cold chemistry; reaction dynamics are extremely sensitive to the details of potential surfaces, such as reaction barrier height and shape, long-range interactions, and nonadiabatic processes.[11]

Another interesting aspect of cold chemistry is the possibility to control the reaction using moderate external fields.[1,12] The potential surfaces involved in reactions can be shifted with respect to each other via the interaction with magnetic, electric, or optical fields, leading to energy-level crossings that can profoundly change the reaction dynamics and outcome. An excellent example of control in ultracold chemistry with photoassociated molecules has been shown by the group of Jun Ye.[4]

The quest to reach the quantum regime of cold chemistry has been hampered by the difficulty of controlling the translational motion of molecules. Laser cooling is based on a favorable electronic level structure that allows closing an optical transition, which is typically not possible with molecules due to their complex internal level structure [an exception to this rule was recently shown for a specific diatomic molecule by J. F. Barry et al. (*Phys. Rev. Lett.* **2012**, *108*, 103002)]. Another method is therefore needed to make the first large step between room temperature and the range of 1 K. In fact, a very cold source of atoms and molecules, the supersonic beam, has been used in molecular physics and chemical physics for more than half a century.[13] This technology has advanced over the years, and beam temperatures as low as 50 mK have been demonstrated with pulsed supersonic valves, such as the Even−Lavie valve.[14] Despite these impressive advances, not a single reaction has been measured at 1 K or below with a neutral species. To explain this surprising fact, we turn to the classic crossed-beam experiments developed by Lee, Herschbach, and collaborators[15] that revolutionized our understanding of reactive dynamics. In those experiments, the collision temperature is defined by the relative velocity of two beams crossing at some angle. During an adiabatic expansion, beams accelerate and reach velocities in the range of several hundred to thousands of meters per second. Even with small crossing angles, the relative velocity remains too high to reach the quantum domain. For example, the lowest temperature achieved so far in a crossed-beam experiment is 23 K in the S + H_2 reaction.[5] However, the collision energy strongly depends on the reduced mass. For a slightly heavier reduced mass of the O + OH reaction (a key interstellar reaction), the same relative velocity as achieved in the S + H_2 collision corresponds to a much higher temperature of 100 K. Interestingly, the lowest temperature achieved to date in neutral species reactive scattering is 5.8 K and was measured with CRESU (Cinétique de Réaction en Ecoulement Supersonique Uniforme) apparatus.[16,17] This was a tour de force experiment that cleverly takes advantage of temperatures that

Special Issue: 2012 Ultracold Molecules

Received: December 6, 2011
Published: July 24, 2012

 © 2012 American Chemical Society dx.doi.org/10.1021/cr2004597 | *Chem. Rev.* 2012, 112, 4879−4889

can be achieved within a single supersonic beam.[5] CRESU gives a very reliable measure of reaction rate at a single temperature point. Inherently there is no possibility to measure the reaction rate as a function of energy with higher energy resolution. This is because the colliding molecule population is distributed among several quantum levels, according to the temperature, and there is no access to reaction products (precluding measurement of differential cross sections).

Many groups realized that cold chemistry (~1 K) can be reached with high-intensity cold supersonic beams if the beam can be decelerated. Several deceleration methods are available such as Stark,[18−20] Zeeman,[21,22] optical,[23] and mechanical.[24,25] Buffer-gas cooling methods[26] and related techniques have also been developed and are able to produce cold beams of molecules and atoms.[27] Experiments with decelerated beams started to appear recently, but all of them investigate inelastic collisions with no reactions reported so far.[28−31] One of the reasons is that barrierless reaction rate constants (usually in the range of 10^{-10}−10^{-13} cm^3 $molecule^{-1}$ s^{-1}) place a stringent requirement on a reactant's density in the reaction volume. The typical temperature of a supersonic beam is in the range of ~1 K with a density of ~10^{10} cm^{-3}. However most of the decelerators cannot slow down the whole velocity distribution and pick only a part of it. Additionally, there are loss mechanisms that reduce the deceleration efficiency such as parametric amplification due to alternating focusing and defocusing forces experienced during the deceleration process. Typical densities achieved so far at low to trapping velocities are in the range of 10^8 cm^{-3} in a 3 × 3 × 3 mm^3 volume. Assuming a reaction rate of 10^{-11} cm^3 $molecule^{-1}$ s^{-1} and unit detection efficiency of reaction products, such densities will give count rates of only 2 events/s at 10 Hz repetition rate. Clearly improving efficiency (or acceptance−phase space volume containing the decelerating particles) is one of the most important challenges in the field.

Magnetic deceleration offers many possibilities in reactive scattering at low ~1 K temperatures. Importantly, atoms such as hydrogen, nitrogen, oxygen, and fluorine can be decelerated, allowing investigations of canonical atom−diatomic molecule reactions. Such processes can also be tracked using quantum mechanical calculations that are necessary to correctly describe dynamics at low temperatures. Reaction complexity can be gradually increased by moving to a larger number of atoms involved, as shown in the following reaction progression that is important to atmospheric and interstellar chemistry: O + OH (3 atoms), F + NH_2 (4 atoms), CN + NO_2 (5 atoms), and NH_2 + NO_2 (6 atoms).

The first demonstrations of magnetic deceleration were reported in 2007 by two groups in parallel. The Merkt group at ETH decelerated atomic hydrogen and deuterium[21,32,33] and the Raizen group at UT Austin decelerated metastable neon.[22,34] Later, the Merkt group reported trapping of atomic hydrogen[35] and deuterium,[36] and the Raizen group decelerated a molecular radical, molecular oxygen.[37] An atomic and molecular coilgun, or equivalently called multistage Zeeman decelerator, operates in analogy with a phase space-stable Stark decelerator.[18] A new type of magnetic decelerator that traps particles in a comoving magnetic trap was proposed earlier[38] and recently realized by the Narevicius group at WIS.[39,40] We will review the progress in the magnetic deceleration and present the state of the art in the field.

2. PHASE-STABLE MAGNETIC DECELERATION

The operational principle of magnetic deceleration is based on the interaction of paramagnetic particles with time-dependent magnetic fields. Paramagnetic particles in the low-field seeking states experience a positive Zeeman shift and are repulsed by high magnetic fields. Such a particle traveling along the axis of an energized electromagnet will "climb" the magnetic field barrier, losing kinetic energy in the process (see Figure 1 a and b). At some point in time, while the particle is on the slope of the magnetic barrier, the magnetic field is switched off suddenly and the particle loses an amount of kinetic energy equal to the Zeeman shift at the switching point (Figure 1 c). Because a supersonic beam has a finite velocity distribution, faster particles will experience higher Zeeman shifts and will lose more kinetic energy relative to the slower particles. Overall the particles remain bunched together throughout the deceleration within this simplified one-dimensional model. Although the deceleration principle in the longitudinal coordinate is analogous to the Stark decelerator, there are substantial differences in the transverse, radial coordinate. In the Stark decelerator, the transverse field gradient sign alternates from stage to stage, changing from focusing to weak defocusing. In magnetic deceleration, there is a very strong focusing force near the center of the solenoid with focusing becoming weaker and finally changing sign to become a weak defocusing force at the entrance to the solenoid (see Figure 3 a and b). At high velocities the effect of strong focusing is beneficial; however, at lower velocities the focusing may become a problem by deflecting trajectories and causing particles to crash into the solenoid surface. To overcome this problem, one has to either reduce the transverse field gradient (for example, by making the solenoid radius larger) or change the location where the magnetic fields are being switched off. Both solutions come at the expense of decreased number of particles or decreased

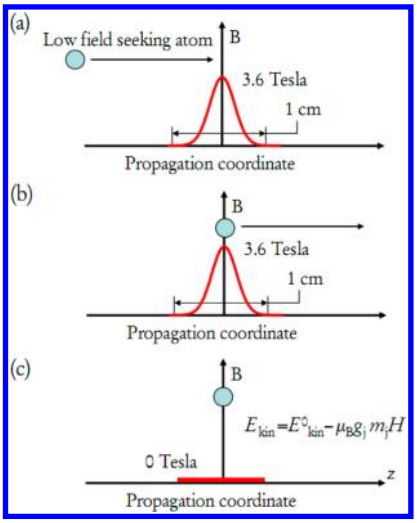

Figure 1. Descriptive diagram of the slowing process. In (a) we see the atom entering the coil, and as it does so it must climb a magnetic "hill". Part (b) shows the atom at the center of the coil with the coil still on, when it has maximized its potential energy. Part (c) shows the atom in the center of the coil with the field switched off. On the right is the equation showing how much kinetic energy would be lost with an ideal coil. Reproduced with permission from ref 34. Copyright 2007 Institute of Physics.

dx.doi.org/10.1021/cr2004597 | Chem. Rev. 2012, 112, 4879−4889

decelerator acceptance, phase space volume that contains the decelerating particles.

Acceptance is a convenient parameter that characterizes the efficiency of the deceleration process. One tries to match the phase space volume of the decelerating beam with that of the supersonic source (mode matching). In the case of phase-space stable deceleration, the highest longitudinal acceptance will be achieved by increasing the peak magnetic field value. The transverse acceptance will be proportional to the focusing force of a solenoid. Both parameters can be experimentally increased by reducing the volume of a solenoid. In the atomic and molecular coilgun, the electromagnets have a bore size of 3 mm with 30 copper windings (0.5 mm wire diameter). Each solenoid is encased between two Permendur disks (10.2 mm diameter, 3 mm thickness) and surrounded by a magnetic steel tube (inner diameter 10.2 mm, outer diameter 17.8 mm, length 9.6 mm; see Figure 2 for details). The high magnetic saturation value of Permendur enables a 25% increase in the peak magnetic field value achieved in the solenoid.

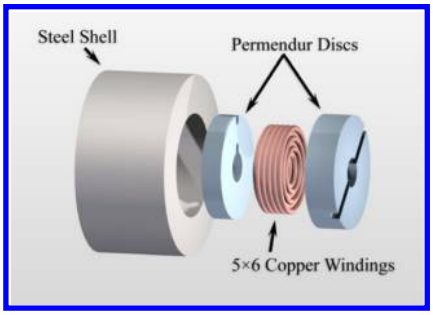

Figure 2. Schematic expanded view of our electromagnetic coils. The bore diameter is 3 mm, and the axial length is also 3 mm. Reproduced with permission from ref 34. Copyright 2007 Institute of Physics.

It is very helpful to know the spatial and temporal behavior of the magnetic fields generated by the solenoids. A convenient method used to characterize the time-dependent magnetic fields generated in the coilgun is based on the Faraday effect.[17] Magneto-optical materials, such as a terbium gallium garnet (TGG) crystal, rotate the polarization of light by an amount proportional to the magnetic field parallel to the light propagation direction. Monitoring the polarization plane rotation of a linearly polarized laser beam and using different length TGG crystals, we calculated a peak field of 5.2 ± 0.2 T in the center of the coil. The switching profile follows an initial exponential rise with a time constant of 19 μs. When we switch off the current, the magnetic field falls linearly to 20% of its peak value in 6 μs. After this linear falloff, the field decays exponentially with a time constant of 17 μs due to eddy currents induced in the Permendur disks by the rapidly changing field. The effect of eddy currents is partially reduced by a current counterpulse (see Figure 4). The magnetic of field

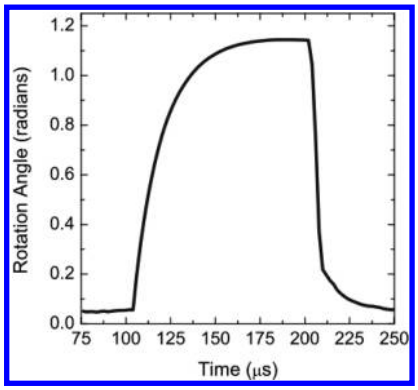

Figure 4. Rotation of the plane of polarization of a HeNe laser passing through a 1.4 mm TGG crystal placed in the bore of a pulsed coil as a function of time. The curve is an average of 200 individual measurements. Reproduced with permission from ref 37. Copyright 2008 American Physical Society.

5.2 T corresponds to the current pulse peaking at 750 A. In our first-generation coilgun, we pulsed 400 A with the magnetic field reaching a peak value of 3.6 T. The transverse magnetic field "well" depth at the top of the magnetic barrier is 0.55 T deep (at 750 A). However, the field gradient varies strongly across the magnetic barrier slope (see Figure 3 b); it is strongest near the top and decreases further away from the center. We can approximate the transverse potential by taking time-averages over several deceleration stages. As a result, the average magnetic field depth becomes 0.2 T.

Now we can easily estimate the phase space volume that contains decelerating particles. In the longitudinal dimension, accepted velocities are ± 8 m/s within 4 mm, and radially accepted velocities are 8 m/s within a 1.5 mm radius. The upper limit of the 6D acceptance is 10^5 $(m/s)^3$ mm^3. The

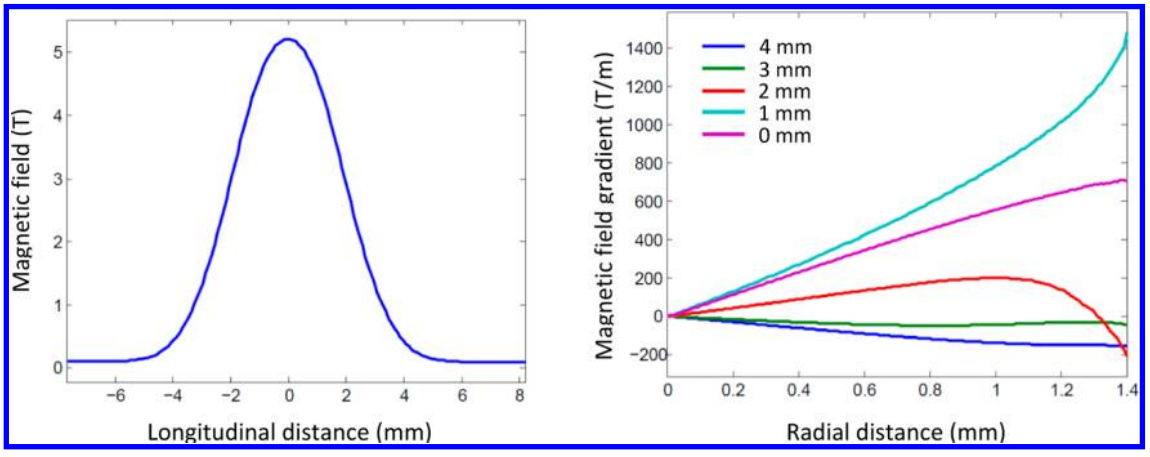

Figure 3. Finite element calculated longitudinal magnetic field (a) and radial magnetic field gradient (b) at different longitudinal positions created in a coilgun solenoid presented in Figure 2.

dx.doi.org/10.1021/cr2004597 | Chem. Rev. 2012, 112, 4879–4889

acceptance is estimated for the case of metastable neon in $^3P_2$ fully stretched, $m_J = 2$, Zeeman sublevel. This estimation holds if the longitudinal oscillation frequency is large compared with the transverse oscillation frequency. At low velocities this approximation breaks down, and effects of overfocusing become detrimental to the deceleration process.

Even at 5.2 T, the amount of kinetic energy removed per stage is small relative to the initial kinetic energy, and many deceleration stages are necessary to stop a supersonic beam traveling at hundreds of meters per second. The large number of deceleration stages requires special care in designing the electronic drivers that provide high current pulses to the solenoids. High-power insulated gate bipolar transistors (IGBTs) are readily available; however, complexity and costs accumulate rapidly with increasing number of channels. The coilgun electronics are simplified by using only 8 high-power IGBTs that switch currents for a number of solenoids connected in parallel and isolated among themselves by inexpensive thyristors. This idea allows easy scalability for construction of very long decelerators without changing the number of expensive high-power IGBTs. Let us describe the coilgun apparatus that was used in the Austin experiments[22,37] in more detail (Figure 5). The starting point of the deceleration

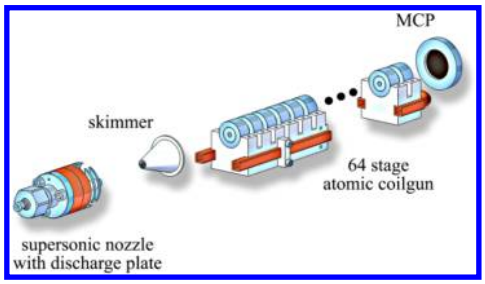

Figure 5. Descriptive drawing of our apparatus. Objects are to scale, but the distances between them are not. Reproduced with permission from ref 22. Copyright 2008 American Physical Society.

experiment is the Even−Lavie supersonic valve. This valve is able to produce intense and cold supersonic beams with an opening time of only 20 μs fwhm (full width at half-maximum). The first experiments reported with the coilgun decelerator were performed on metastable neon.[22] Metastable neon was created at the orifice of the supersonic nozzle by a dc discharge that excited neon atoms into the $^3P_2$ long-lived metastable electronic state. The magnetic moment in this state is 3 Bohr magnetons (μ_B). The mass-to-magnetic moment ratio in the fully stretched level is 6.6 amu/μ_B and is close to the ratio found in molecular radicals in their electronic ground states such as OH (8 amu/μ_B) or NH (5 amu/μ_B). As such, metastable neon is a convenient test case allowing characterization of the deceleration process and with the possibility of comparing results with the Stark deceleration. After traveling 250 mm the supersonic beam reaches a 50 mm long, 5 mm orifice diameter skimmer and continues to the first stage of the coilgun decelerator, which is mounted 250 mm from the skimmer base. The solenoids are fixed on a monolithic aluminum structure that serves as both a heat sink and an alignment fixture. Because of the small solenoid bore diameter (3 mm), the coils are placed inside the vacuum chamber, and electrical connections are made using a large number of electrical feedthroughs. The detection of metastable neon atoms emerging from the decelerator is done using a multichannel plate (MCP) detector. Because the beam velocity varies during deceleration, it is impossible to extract the decelerated beam velocity and spread using a single time-of-flight trace. The problem can be overcome by mounting the MCP detector on a traveling stage that allows several time-of-flight traces to be measured. This method provides a direct measurement of both beam velocity and velocity distribution width (or beam temperature).

The final velocity depends on the position of an atom at the time the magnetic fields are switched off. Atoms close to the solenoid center experience a larger Zeeman shift and lose a larger amount of kinetic energy. Although switching closer to the top of the magnetic barrier removes more energy, it comes at the price of decreased atom number. Because of the finite velocity spread, atoms that are faster than the target atom (synchronous atom, following the Stark decelerator definitions) can reach the falling slope of the magnetic field barrier and start accelerating out of the solenoid. It is thus clear that the highest efficiency (or acceptance) for the coilgun decelerator is expected for a switching sequence that takes place at the middle of the magnetic potential barrier. One could argue that the acceptance will be even higher if switching is done at the lower half of the potential barrier; however, in this case particles experience a defocusing force at the entrance of a solenoid, reducing the acceptance.

The prototype of the coilgun, consisting of 18 stages with the peak magnetic field of 3.6 T, was used to decelerate metastable neon from 460 to 400 m/s. The next step was the construction of a 64-stage coilgun with increased magnetic field of 5.2 T. We present the experimental results for deceleration of metastable neon in Figures 6 and 7. The initial beam velocity was 446.5 m/

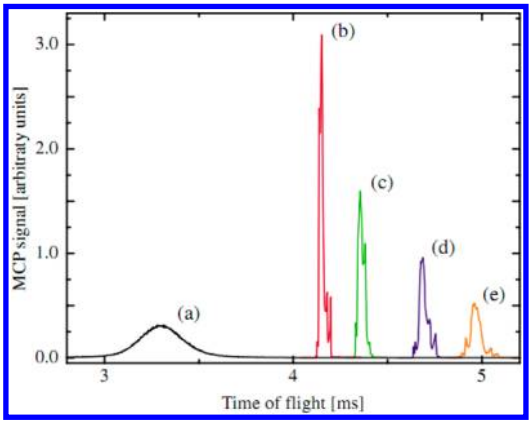

Figure 6. Time-of-flight measurements recorded with the MCP detector for different phases, along with a reference beam (a). Each curve is an average over 20 shots at a repetition rate of 0.075 Hz. The slowed curves show only the slowed portion of the beam for clarity. Beam velocities are (a) 446.5 m/s, (b) 222 m/s, (c) 184.7 m/s, (d) 142.7 m/s, and (e) 109.9 m/s. Reproduced with permission from ref 22. Copyright 2008 American Physical Society.

s and the beam was decelerated to 55.8 m/s, removing >98% of the initial kinetic energy. There are a few interesting points one can observe in the experimental traces. The decelerated beams show a structure in the time-of-flight signal. This is a direct result of anharmonicity of the magnetic fields that causes atoms to oscillate longitudinally with different frequencies. The efficiencies range from 11.9% to 2% for the slowest peak. Taking into account that only the fully stretched component is

dx.doi.org/10.1021/cr2004597 | Chem. Rev. 2012, 112, 4879–4889

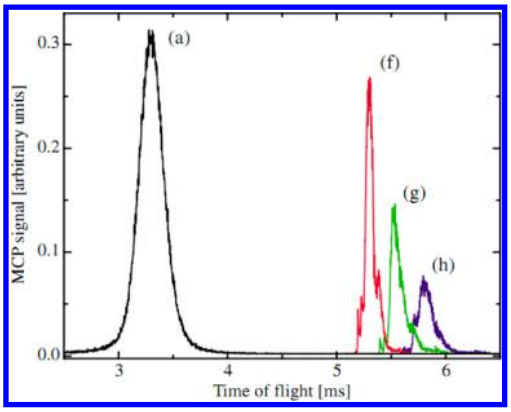

Figure 7. Time-of-flight measurements recorded with the MCP detector for different phases along with a reference beam (a). Each curve is an average over 20 shots at a repetition rate of 0.075 Hz. The slowed curves show only the slowed portion of the beam for clarity. Beam velocities are (a) 446.5 m/s, (f) 84.1 m/s, (g) 70.3 m/s, and (h) 55.8 m/s. Reproduced with permission from ref 22. Copyright 2008 American Physical Society.

being decelerated, 2% efficiency corresponds to ~10% of atoms in the $m_J = 2$ state that reach the first coil.

The coilgun was also used to magnetically decelerate molecular oxygen,[37] the first demonstration of magnetic deceleration with a molecular species. The experimental apparatus was similar to that used in metastable neon deceleration with the difference that a quadrupole mass spectrometer (QMS) was used to detect the molecular oxygen. The initial beam velocity was 389 m/s, achieved by using a 1:5 oxygen/krypton gas mixture cooled to 148 K. A final velocity of 83 m/s was reached, removing 95% of the initial kinetic energy (presented in Figure 8).

The coilgun design is optimized for beam deceleration and not trapping. At lower velocities it is harder to keep particles bunched together because of strong transverse gradients. One solution is to decrease the transverse magnetic field gradient by increasing the solenoid length and inner diameter as was done

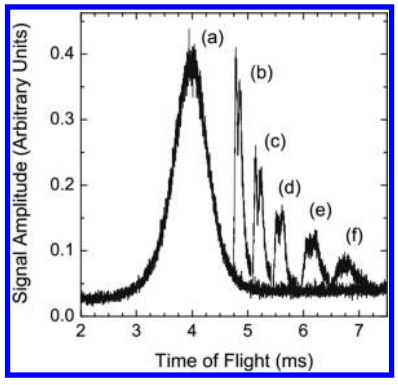

Figure 8. Time-of-flight measurements of molecular oxygen recorded with the QMS detector for different phases along with a reference beam. The slowed curves show only the slowed portion of the beam for clarity. Beam velocities are (a) 389 m/s, (b) 242 m/s, (c) 195 m/s, (d) 155 m/s, (e) 114 m/s, and (f) 83 m/s. Each profile is an average of 200 individual measurements. The ratio of the area under each slow peak to the geometrically scaled area under the reference beam (at the position of the first slower coil) is (b) 2.3%, (c) 1.7%, (d) 1.2%, (e) 1%, and (f) 0.8%. Reproduced with permission from ref 37. Copyright 2008 American Physical Society.

in atomic hydrogen and deuterium trapping experiments. However, it will strongly reduce the transverse and longitudinal acceptance because both effective transverse and longitudinal potential wells become shallower.

The Zeeman decelerator developed at ETH follows the approach of increased solenoid volume with smaller focusing forces, beneficial for deceleration of particles with smaller mass-to-magnetic moment ratio. The solenoid dimensions used in the first experiment that demonstrated deceleration of atomic hydrogen[21] were 5 mm bore diameter, 7.8 mm length, and 21 windings of 300 μm wire. The peak magnetic field was ~1 T. Atomic hydrogen guiding and deceleration time-of-flight data are shown in Figure 9. In the case of the Zeeman decelerator, there is a possibility that atoms will pass through a zero magnetic field, causing Majorana spin flips. The effect has been studied in detail,[32] and it has been shown that it can be avoided by overlapping successive current pulses.

The Zeeman decelerator peak magnetic field was raised to 1.55 T, and slow beams of atomic hydrogen[33] (see Figure 10) and deuterium[32] were generated. Later, the Merkt group constructed a magnetic quadrupole trap at the exit of a 12-stage Zeeman decelerator. Trapping of atomic hydrogen[35] and deuterium[36] was demonstrated using this setup (see Figures 11 and 12 for results).

The Zeeman decelerator acceptance has been studied,[41] showing an interesting interplay between the focusing and defocusing for different phase angles. At higher phase angles and higher final velocities, particles experience mostly focusing forces, and losses due to parametric amplification are suppressed as shown in Figure 13. However, lower focusing gradient and overall smaller peak magnetic field reduce the acceptance of the Zeeman decelerator. The Zeeman decelerator acceptance for the case of metastable neon is estimated to be 2×10^3 mm^3 (m/s)^3,[42] and the upper limit for the acceptance of the coilgun decelerator is 10^5 mm^3 (m/s)^3. For comparison, the acceptance of the conventional Stark decelerator at 50 m/s final velocity is 3×10^4 mm^3 (m/s)^3.[43] With such an acceptance, the reaction product detection is limited to only the fastest processes. To be able to observe cold reactive chemistry with a decelerated crossed-beam arrangement, one needs to improve the performance of decelerators. This must be done by increasing the acceptance to a level that will match the emittance of a supersonic beam source.

The acceptance at low final velocities can be dramatically increased using a different approach to beam deceleration. As was suggested,[38] the supersonic beam could be decelerated in a traveling magnetic trap, overcoming issues with transverse confinement altogether. The electrostatic analogue of this idea has been demonstrated both on a microchip[19] and with an array of macroscopic ring electrodes.[20]

3. MOVING MAGNETIC TRAP DECELERATOR

The Narevicius group has recently demonstrated that deceleration in a moving trap is especially beneficial at trapping velocities (below 100 m/s), giving an advantage of over 2 orders of magnitude in the phase space volume that contains slowed particles as compared to other techniques.[39,40] Also, the magnetic trap 6D phase space volume reported in refs 39 and 40 matches the emittance of the supersonic source, allowing deceleration of light radical molecules and most atoms, limited only by the distribution among low field seeking states within the Zeeman sublevel structure. The moving magnetic trap deceleration idea was inspired by the atom conveyor belt that

dx.doi.org/10.1021/cr2004597 | Chem. Rev. 2012, 112, 4879–4889

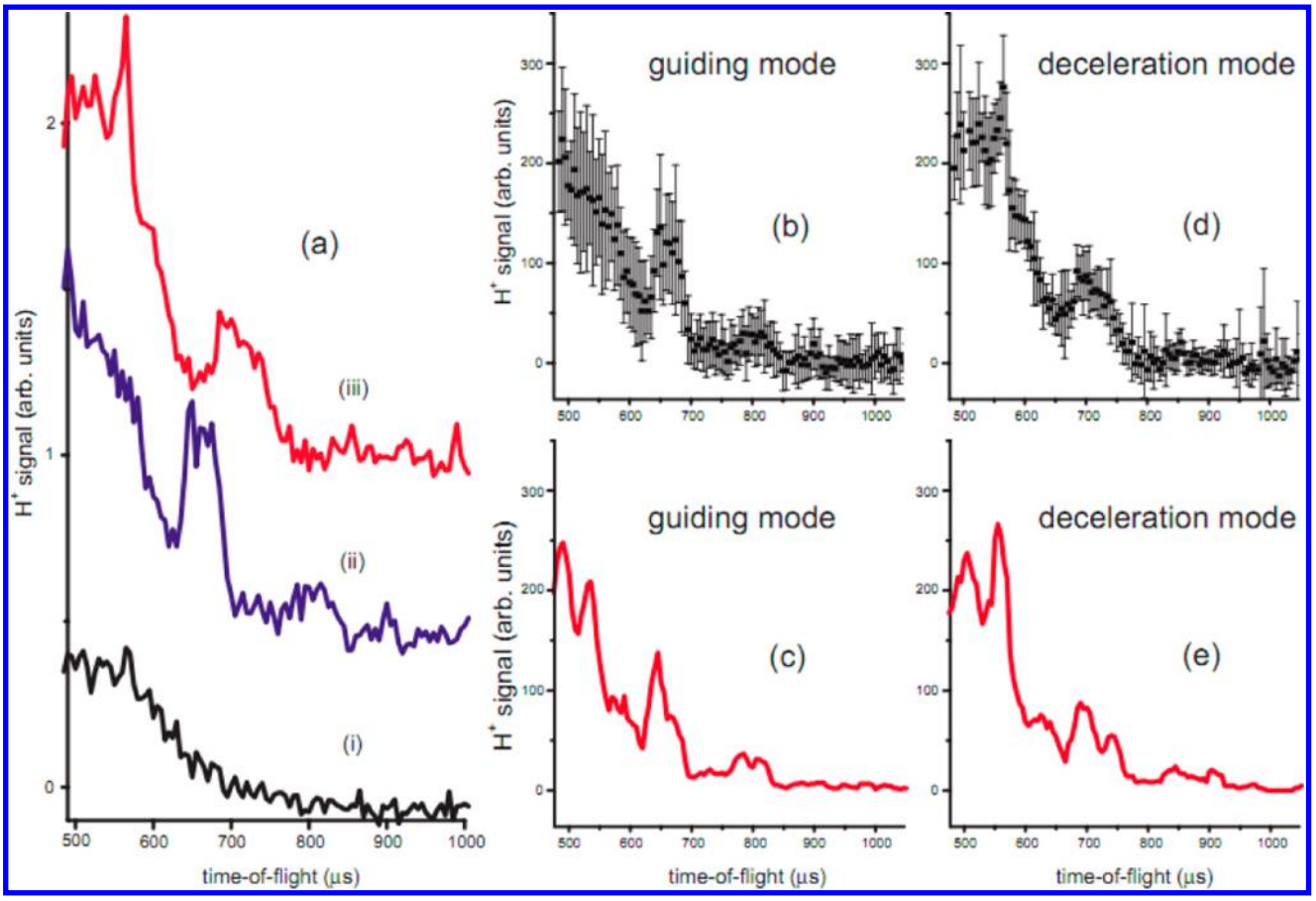

Figure 9. (a) Measured time-of-flight profiles of a beam of H atoms in the $^2S_{1/2}$ ground state passing through the Zeeman decelerator: (i) decelerator kept off, (ii) decelerator operating in a guiding mode at 313 m/s, and (iii) decelerator operating to slow down H atoms from 313 m/s down to 225 m/s. For the sake of clarity, measured profiles are given an offset but are all on the same vertical scale. (b and [d]) Measured time-of-flight profiles of H atoms after passing through the decelerator operating in the guiding mode at 313 m/s [decelerating from 313 m/s down to 225 m/s], including experimental error bars (1 standard deviation). (c and [e]) Output of a trajectory simulation using the same guiding [decelerating] time sequence. Reproduced with permission from ref 21. Copyright 2007 American Physical Society.

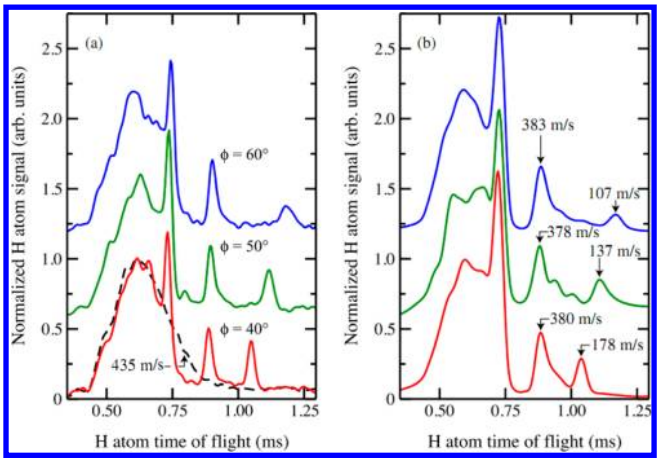

Figure 10. H atom time-of-flight profiles measured at the end of the multistage Zeeman decelerator following deceleration at three different phase angles, 40°, 50°, and 60°. (a) Experimental results. The dashed line represents the time-of-flight profile of the undecelerated beam. (b) Simulations. The velocities indicated above the traces were obtained from the simulations. Reproduced with permission from ref 33. Copyright 2008 Institute of Physics.

has been successfully used to transport atoms on microchips[44] or across centimeter-long distances in cold atom experiments.[45]

An effective moving magnetic trap potential was created using a series of spatially overlapping traps and activating them in a temporally overlapping pulse sequence (see Figure 14 a and b). Each trap consists of two coils in an anti-Helmholtz configuration (quadrupole trap and is axially shifted from the next trap by half the coil-to-coil distance. Once the magnetic field in a given trap reaches the maximal value, the adjacent trap is gradually switched on and the magnetic field minimum shifts to its new position in the center of the next trap. The center-to-center distance between the coils forming a single trap is 10.4 mm with a bore diameter of 10.2 mm. The quadrupole coils configuration is not symmetric; one coil has 16 windings whereas the second coil has 8, both of a 0.46 mm diameter copper wire. With 500 A peak current pulse, the "front" and "back" barrier heights reach 1 and 0.4 T, respectively. During deceleration, a fictitious force tilts the effective potential such that the "back" barrier height increases whereas the "front" barrier height decreases, making the moving trap symmetric in the decelerating frame of reference. Magnetic field profiles, both temporal and spatial, were characterized using the Faraday effect and are shown in Figure 14c. The overlap time between two consecutive current pulses defines the velocity of the trap at different slowing stages. To decelerate the moving trap, the overlap time has to be gradually increased. The pulse length is controlled by an electronic driver based on an LCR circuit.

dx.doi.org/10.1021/cr2004597 | Chem. Rev. 2012, 112, 4879–4889

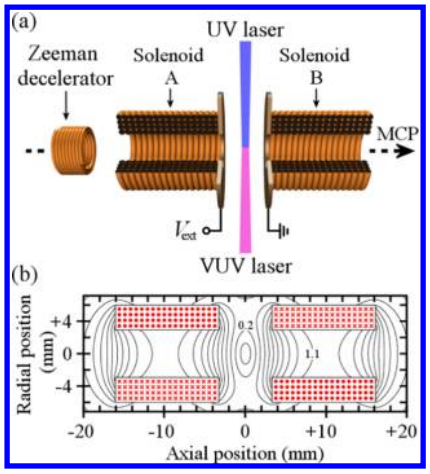

Figure 11. (a) Schematic diagram of the quadrupole trap. The H atom beam propagates from left to right and after exiting the 12-stage decelerator enters the two solenoids (labeled A and B) that form the trap. Atoms in the trap volume are detected by VUV + UV two-photon excitation to Rydberg states followed by pulsed electric field ionization. H^+ ions are then extracted through solenoid B to the MCP detector (not pictured). (b) Distribution of magnetic field strength in the plane containing the axis of symmetry of the quadrupole trap for currents of 200 A applied to each solenoid. The contours of constant magnetic field strength are drawn in steps of 0.1 T. Reproduced with permission from ref 35. Copyright 2008 American Physical Society.

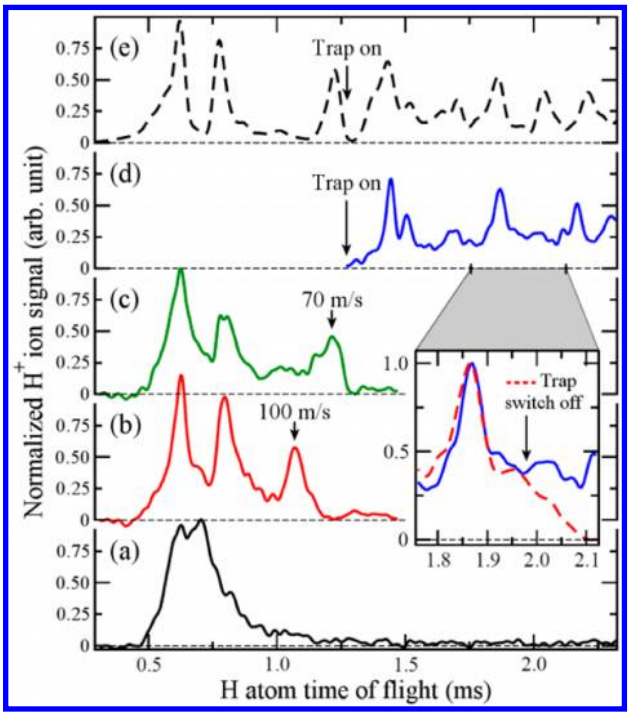

Figure 12. TOF profiles of the H atom beam (a) with the decelerator off, (b) with the 12-stage decelerator on but with the trap solenoids off, (c) after deceleration with the decelerator and the first trap solenoid. (d) Detection of trapped atoms after switching on the trap. (e) Simulation of the experimental results. The inset is an expanded view of part of trace (d) along with the signal measured when the trap is switched off at 1.98 ms (dashed curve). Reproduced with permission from ref 35. Copyright 2008 American Physical Society.

Each quadrupole coil is connected in series with a "binary tune box" (BTB) of inductors, which allows one to control the LCR inductance with a resolution of 1 μH. The BTB is composed of

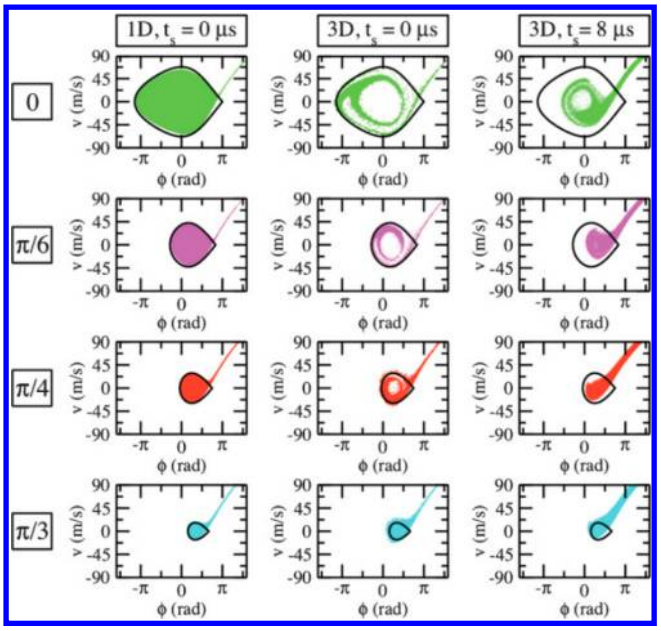

Figure 13. Comparison of the one-dimensional phase-stability model with particle-trajectory simulations for selected values of phase (increasing from top to bottom). Left and middle columns: one- and three-dimensional particle-trajectory simulations assuming instantaneous switch-off of the current (i.e., ts = 0), respectively. Right column: Three-dimensional particle-trajectory simulations taking into account the ts = 8 μs switch-off time of the currents. The bold line in each graph shows the separatrix derived using one-dimensional model. Reproduced with permission from ref 41. Copyright 2010 American Physical Society.

6 inductors (2^0, 2^1, ..., 2^5 μH) connected in series and bypassed with power transistors that are used to set the auxiliary inductance that changes the LCR circuit (inductor, capacitor resistor circuit) time constant.

The comoving trap decelerator apparatus is shown schematically in Figure 15. The supersonic beam of metastable neon was created using dielectric barrier discharge mounted near the orifice of an Even–Lavie valve[14] cooled to 74 K. A conical skimmer with a 4 mm orifice diameter is placed 15 cm from the valve. The deceleration begins 14 cm after the skimmer. The decelerator consists of 213 overlapping quadrupole traps extending over 114 cm. The last 161 traps are encased in Permendur, a material with high saturation magnetization, which increases the magnetic field by 20%. As the atoms exit the deceleration region, they propagate freely 1.4 cm until reaching a microchannel plate (MCP) detector. The detector is mounted on a moving stage capable of a 5.2 cm axial translation.

A supersonic beam of metastable neon was decelerated from an initial velocity of 429.7 ± 6.0 m/s (trace a in the inset of Figure 16A) to eight different final velocities. The standard deviation of the initial beam is 11.2 m/s corresponding to a temperature of 302 mK in the moving frame of reference. In Figure 16A, eight decelerated peaks (traces c–j) and a guided peak (no deceleration, Figure 16A, trace b) are shown. In Figure 16B, Monte Carlo simulations of the decelerator performance, calculated under the same experimental conditions, are included as well.

The guided beam peak intensity is larger compared to the intensity of the free flight beam. This is a direct result of the three-dimensional confinement, leading to a higher number of

dx.doi.org/10.1021/cr2004597 | Chem. Rev. 2012, 112, 4879–4889

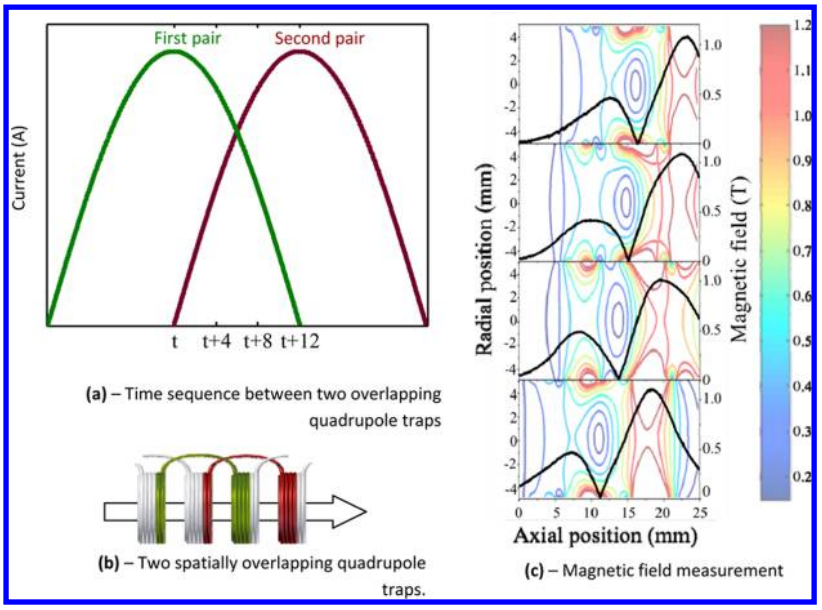

Figure 14. (a) Time sequence between two overlapping quadrupole traps. Each pulse behaves as half a sine wave with duration of 24 μs. (b) Two quadrupole traps spaced by 5.2 mm. (c) Magnetic field measurement. Black solid lines are the snapshots of the axial magnetic field as measured during the magnetic trap movement. The contour plots represent the magnetic fields as calculated by finite element simulation. Reproduced with permission from ref 39. Copyright 2011 Royal Society of Chemistry.

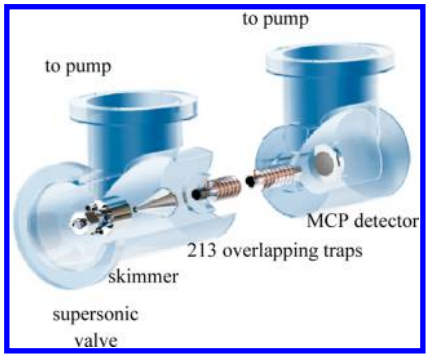

Figure 15. Schematics of our experimental apparatus. Objects are to scale; however, the distances between them are not. Reproduced with permission from ref 40. Copyright 2011 Institute of Physics.

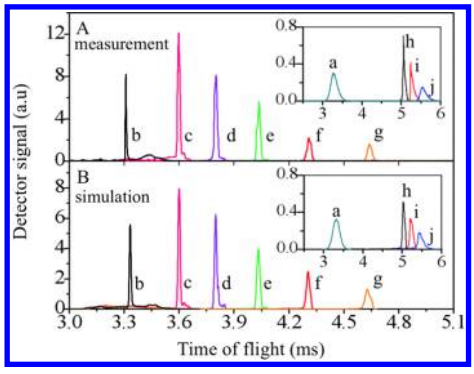

Figure 16. Time-of-flight measurements (A) and Monte Carlo simulation results (B) of supersonic beam decelerations of metastable neon from an initial velocity of 429.7 ± 6.0 m/s (a—inset) to final velocities: guiding at 432.3 ± 3.6 (b), 352.5 ± 4.2 m/s (c), 298.6 ± 2.2 m/s (d), 249.2 ± 1.6 m/s (e), 199.4 ± 1.2 m/s (f), and 148.4 ± 0.8 m/s (g). Inset: lower final velocities: 97.9 ± 1.0 m/s (h), 76.0 ± 1.6 m/s (i), and 53.8 ± 1.1 m/s (j). The simulation was normalized to the data peak area at the final velocity of 97.9 m/s. Reproduced with permission from ref 40. Copyright 2011 Institute of Physics.

atoms reaching the detector in a shorter time. Another interesting observation is that the area of the peak that corresponds to 352 m/s (c) is larger than the one of the guided beam (b). This is attributed to the change in the dimensions of the trap as a function of deceleration value.

The moving magnetic trap decelerator acceptance was established by performing numerical Monte Carlo simulations (with no free parameters) with magnetic fields calculated using a finite-element method. In Figure 17, the calculated longitudinal and transverse phase space distributions are shown for two final velocities, 350 m/s (Figure 17A and B) and 50 m/s (Figure 17C and D). The solid lines in Figure 17A and C represent separatrices calculated using the one-dimensional time-averaged longitudinal potential, including

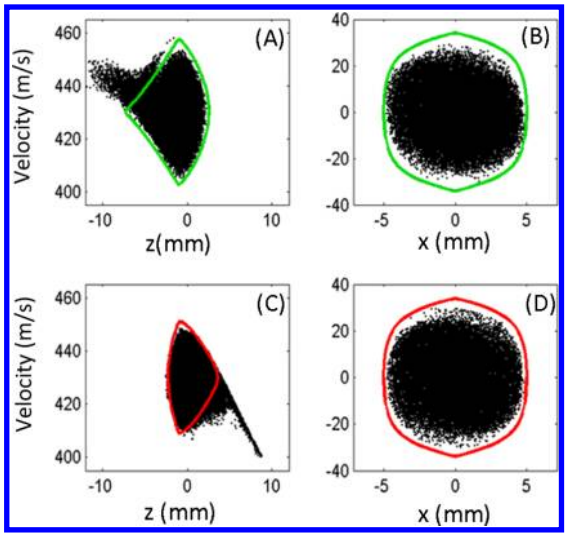

Figure 17. Longitudinal and transverse phase space distributions along with one-dimensional separatrices for 350 m/s (A and B) and 50 m/s (C and D) final velocities.

dx.doi.org/10.1021/cr2004597 | *Chem. Rev.* 2012, 112, 4879–4889

the tilt due to the fictitious force. The transverse phase space distributions are shown in Figure 17B and D along with separatrices constructed using the one-dimensional time-averaged transverse potential. As one can see, the simple one-dimensional model captures the main features of the moving magnetic trap decelerator performance. The maximum calculated acceptance of the moving magnetic trap decelerator was estimated to be above 1×10^7 $(mm)^3$ $(m/s)^3$ and is obtained for a deceleration value of 50 000 m/s^2 (2.9 ms deceleration time) to the final velocity of 50 m/s.[39] Importantly, the optimal acceptance of decelerator is very close to the emittance of the supersonic source, estimated to be $\sim 6 \times 10^6$ mm^3 $(m/s)^3$ (at a distance of 15 cm from the valve, assuming a longitudinal velocity spread of $\pm$11 m/s and a 5 mm diameter skimmer 10 cm from the valve). Mode matching between the source and the moving magnetic trap can be easily achieved with such a configuration.

In a different approach, Vanhaecke et al. created a traveling magnetic wave with the help of a helical wire arrangement with additional quadrupole coils to ensure transverse confinement. This group recently showed guiding of a metastable argon beam.[46] The frequency of this traveling magnetic wave can be chirped in order to decelerate the trapped supersonic beam, although this was not yet demonstrated experimentally. A schematic picture of the experimental setup with guiding results is shown in Figures 18 and 19.

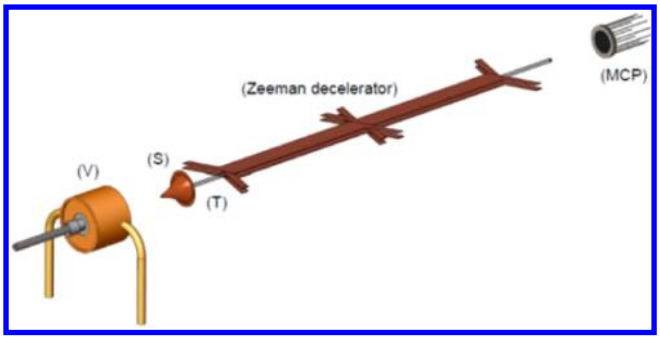

Figure 18. Schematic representation of the experimental setup. The production chamber contains the valve (V) and the skimmer (S) while the detection chamber hosts the detector (MCP). The beam passes from the production chamber to the detection chamber through a 400-mm-long glass tube (T). The coils (Zeeman decelerator), i.e., the flat coils and the quadrupole coils, are mounted outside vacuum, around the tube (T). Reproduced with permission from ref 46. Copyright 2011 Springer Science.

4. SUMMARY

Magnetic deceleration for neutral atoms and molecules is a relatively new technique but in a short time has been able to reach phase space volumes that will enable the study of cold chemistry in the laboratory. Future improvements include the optimization of mode-matching of the supersonic source to the moving magnetic trap and mode-matching to the final stage of a static magnetic trap containing multiple species of atoms and molecules.

A magnetic moving trap decelerator offers a unique and interesting application toward studying cold chemistry. Different than the conventional Zeeman or coilgun decelerators that serve also as mass-to-magnetic moment filters, the moving trap decelerator can easily decelerate and trap mixtures of atoms and molecules having different mass-to-magnetic moment ratios.

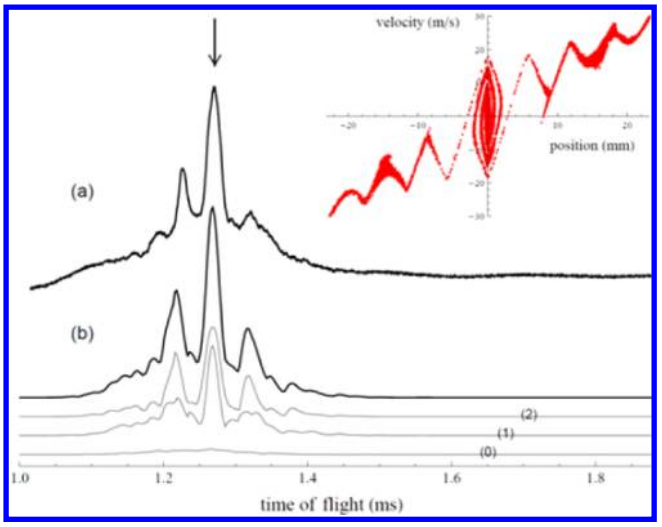

Figure 19. (a) Experimental time-of-flight of a beam of metastable argon atoms subject to a magnetic wave traveling at 464 m/s. The pronounced peak at 1.270 ms consists of atoms that have been trapped at a node of the traveling wave. (b) Three-dimensional simulation of the experiment. The curve (0) (respectively (1), (2)) represents the contribution to the time-of-flight profile by the atoms in the $M_J = 0$ (respectively, $M_J = 1$, $M_J = 2$) magnetic sublevel of the $^3P_2$ state. The inset displays a snapshot of the phase space distribution of the atoms of the beam, taken 800 μs after the atom cloud has left the nozzle. Reproduced with permission from ref 46. Copyright 2011 Springer Science.

One particularly promising candidate is a mixture of atomic oxygen and a molecular hydroxyl radical, OH, that reacts even at low temperatures to form molecular oxygen and atomic hydrogen. Trapping the mixture in a static magnetic trap will enable an increase in the interaction time by several orders of magnitude, and will enable observation of a chemical reaction that is fundamental to interstellar space studies at temperatures as low as 100 mK.

Additional improvements in phase space volume will require the implementation of cooling methods. One of the most promising approaches is single-photon cooling, which is based on the concept of a one-way wall for atoms or molecules and is a direct realization of Maxwell's Demon. This method was demonstrated experimentally with atoms, leading to a 350× increase in phase space volume from a magnetic trap.[47,48] The realization of single-photon cooling of molecules should enable similar improvements[49] and will enable the study of chemical reactions at ultracold temperatures. The coming years promise to be an exciting period, with many novel directions to pursue and hopefully many surprises.

AUTHOR INFORMATION

Corresponding Author

*E-mail: edn@weizmann.ac.il.

Notes

The authors declare no competing financial interest.

dx.doi.org/10.1021/cr2004597 | Chem. Rev. 2012, 112, 4879–4889

Biographies

Edvardas Narevicius earned his Ph.D. in theoretical Quantum Chemistry with Prof. Nimrod Moiseyev at the Technion, Israel Institute of Technology, Haifa, Israel, in 2002. He went to industry and worked as a senior scientist in OpTun Inc. developing optical components and subsystems. He invented an adiabatic mode multiplexer, a key component in many of OpTun's optical devices. He returned to academia joining the group of Prof. Mark G. Raizen at University of Texas at Austin as a postdoc and worked on coilgun decelerator and single-photon cooling projects. Since 2008 he is a senior researcher at the department of chemical physics in the Weizmann Institute of Science and holds the Ernst and Kathe Ascher carrier development Chair. His current interests are focused on cold chemistry with the first experimental observation of quantum effects in cold reactions recently achieved in his group. His group also developed a moving magnetic trap decelerator.

Mark Raizen earned his Ph.D. at the University of Texas at Austin in 1989 under the joint supervision of Prof. Steven Weinberg and Prof. H. J. Kimble. He went on to do a postdoctoral fellowship at the National Institute of Standards and Technology in Boulder, CO, working with Dr. David Wineland. He returned to The University of Texas at Austin in 1991 as an Assistant Professor and was promoted to tenure in 1996 and then to full professor in 2000. He has held the Sid W. Richardson Chair in Physics since 2000. He is a Fellow of the American Physical Society and the Optical Society of America. He was an National Science Foundation and Office of Naval Research Young Investigator, and a Sloan Foundation Fellow. He received the I. I. Rabi Prize of the American Physical Society, the Max Planck Award from the Humboldt Foundation and the Max Planck Society, and the Willis Lamb Medal in Laser Science. Prof. Raizen pioneered the study of quantum chaos with cold atoms. In parallel, he developed a program to study quantum transport phenomena, using cold atoms to study phenomena from condensed matter physics. In the past decade, Prof. Raizen and his group pioneered the development of general methods for cooling and trapping of atoms, applicable to most atoms in the periodic table, as well as certain molecules.

ACKNOWLEDGMENTS

E. N. acknowledges the historic generosity of the Harold Perlman Family and support from the Israel Science Foundation. M. G. R. acknowledges support from the U.S. National Science Foundation, the R.A. Welch Foundation, Grant number F-1258, and the Sid W. Richardson Foundation.

REFERENCES

(1) Bell, M.; P. Softley, T. *Mol. Phys.* **2009**, *107*, 99.
(2) Lincoln, D. C.; DeMille, D.; Krems, V. R.; Jun, Y. *New J. Phys.* **2009**, *11*, 055049.
(3) Willitsch, S.; Bell, M. T.; Gingell, A. D.; Procter, S. R.; Softley, T. P. *Phys. Rev. Lett.* **2008**, *100*, 043203.
(4) Ospelkaus, S.; Ni, K.-K.; Wang, D.; de Miranda, M. H. G.; Neyenhuis, B.; Quemener, G.; Julienne, P. S.; Bohn, J. L.; Jin, D. S.; Ye, J. *Science* **2010**, *327*, 853.
(5) Berteloite, C.; Lara, M.; Bergeat, A.; Le Picard, S.; Dayou, F.; Hickson, K. M.; Canosa, A.; Naulin, C.; Launay, J.-M.; Sims, I. R.; Costes, M. *Phys. Rev. Lett.* **2010**, *105*, 203201.
(6) Smith, I. W. M.; Rowe, B. R. *Acc. Chem. Res.* **2000**, *33*, 261.
(7) Stief, L. J.; Marston, G.; Nava, D. F.; Payne, W. A.; Nesbitt, F. L. *Chem. Phys. Lett.* **1988**, *147*, 570.
(8) Aquilanti, V.; Cavalli, S.; De Fazio, D.; Volpi, A.; Aguilar, A.; Lucas, J. M. *Chem. Phys.* **2005**, *308*, 237.
(9) Dong, W.; Xiao, C.; Wang, T.; Dai, D.; Yang, X.; Zhang, D. H. *Science*, **2006***327*, 1501.
(10) Neumark, D.; Wodtke, A.; Robinson, G.; Hayden, C.; Lee, Y. T. *J. Chem. Phys.* **1985**, *82*, 3045.
(11) Lique, F.; Li, G.; Werner, H.; Alexander, M. H. *J. Chem. Phys.* **2011**, *134*, 231101.
(12) Krems, R. V. *Phys. Chem. Chem. Phys.* **2008**, *10*, 4079.
(13) Campargue, R. *Atom and Molecular Beams: The State of the Art 2000*; Springer: Berlin, 2001.
(14) Even, U.; Jortner, J.; Noy, D.; Lavie, N.; Cossart-Magos, C. *J. Chem. Phys.* **2000**, *112*, 8068.
(15) Lee, Y. T.; McDonald, J.; LeBreton, P.; Herschbach, D. *Rev. Sci. Instrum.* **1969**, *40*, 1402.
(16) Rowe, B. R.; Dupeyrat, G.; Marquette, J. B.; Gaucherel, P. *J. Chem. Phys.* **1984**, *80*, 4915.
(17) Smith, I. W. M. *Angew. Chem., Int. Ed.* **2006**, *45*, 2842.
(18) Bethlem, H. L.; Berden, G.; Meijer, G. *Phys. Rev. Lett.* **1999**, *83*, 1558.
(19) Meek, S. A.; Bethlem, H. L.; Conrad, H.; Meijer, G. *Phys. Rev. Lett.* **2008**, *100*, 153003.
(20) Osterwalder, A.; Meek, S. A.; Hammer, G.; Haak, H.; Meijer, G. *Phys. Rev. A* **2010**, *81*, 051401.
(21) Vanhaecke, N.; Meier, U.; Andrist, M.; Meier, B. H.; Merkt, F. *Phys. Rev. A: At., Mol., Opt. Phys.* **2007**, *75*, 031402.
(22) Narevicius, E.; Libson, A.; Parthey, C. G.; Chavez, I.; Narevicius, J.; Even, U.; Raizen, M. G. *Phys. Rev. Lett.* **2008**, *100*, 093003.
(23) Fulton, R.; Bishop, A. I.; Barker, P. F. *Phys. Rev. Lett.* **2004**, *93*, 243004.
(24) Gupta, M.; Herschbach, D. *J. Phys. Chem. A* **2001**, *105*, 1626.
(25) Strebel, M.; Stienkemeier, F.; Mudrich, M. *Phys. Rev. A* **2010**, *81*, 033409.
(26) Doyle, J. M.; Friedrich, B.; Kim, J.; Patterson, D. *Phys. Rev. A* **1995**, *52*, R2515.
(27) Rangwala, S. A.; Junglen, T.; Rieger, T.; Pinkse, P. W. H.; Rempe, G. *Phys. Rev. A* **2003**, *67*, 043406.
(28) Gilijamse, J. J.; Hoekstra, S.; van de Meerakker, S. Y. T.; Groenenboom, G. C.; Meijer, G. *Science* **2006**, *313*, 1617.
(29) van de Meerakker, S. Y. T.; Meijer, G. *Faraday Discuss.* **2009**, *142*, 113.

(30) Kirste, M.; Scharfenberg, L.; Kłos, J.; Lique, F.; Alexander, M. H.; Meijer, G.; van de Meerakker, S. Y. T. *Phys. Rev. A* **2010**, *82*, 042717.
(31) Sawyer, B. C.; Stuhl, B. K.; Yeo, M.; Tscherbul, T. V.; Hummon, M. T.; Xia, Y.; Klos, J.; Patterson, D.; Doyle, J. M.; Ye, J. *Phys. Chem. Chem. Phys.* **2011**, *13*, 19059.
(32) Hogan, S. D.; Sprecher, D.; Andrist, M.; Vanhaecke, N.; Merkt, F. *Phys. Rev. A* **2007**, *76*, 023412.
(33) Hogan, S. D.; Wiederkehr, A. W.; Andrist, M.; Schmutz, H.; Merkt, F. *J. Phys. B: At., Mol. Opt. Phys.* **2008**, *41*, 081005.
(34) Narevicius, E.; Parthey, C. G.; Libson, A.; Narevicius, J.; Chavez, I.; Even, U.; Raizen, M. G. *New J. Phys.* **2007**, *9*, 358.
(35) Hogan, S. D.; Wiederkehr, A. W.; Schmutz, H.; Merkt, F. *Phys. Rev. Lett.* **2008**, *101*, 143001.
(36) Wiederkehr, A. W.; Hogan, S. D.; Lambillotte, B.; Andrist, M.; Schmutz, H.; Agner, J.; Salathé, Y.; Merkt, F. *Phys. Rev. A* **2010**, *81*, 021402.
(37) Narevicius, E.; Libson, A.; Parthey, C. G.; Chavez, I.; Narevicius, J.; Even, U.; Raizen, M. G. *Phys. Rev. A* **2008**, *77*, 051401(R).
(38) Narevicius, E.; Parthey, C. G.; Libson, A.; Riedel, M. F.; Even, U.; Raizen, M. G. *New J. Phys.* **2007**, *9*, 96.
(39) Lavert-Ofir, E.; David, L.; Henson, A. B.; Gersten, S.; Narevicius, J.; Narevicius, E. *Phys. Chem. Chem. Phys.* **2011**, *13*, 18948.
(40) Lavert-Ofir, E.; Sasha, G.; Alon, B. H.; Itamar, S.; Liron, D.; Julia, N.; Edvardas, N. *New J. Phys.* **2011**, *13*, 103030.
(41) Wiederkehr, A. W.; Hogan, S. D.; Merkt, F. *Phys. Rev. A* **2010**, *82*, 043428.
(42) Wiederkehr, A. W.; Motsch, M.; Hogan, S. D.; Andrist, M.; Schmutz, H.; Lambillotte, B.; Agner, J. A.; Merkt, F. *arXiv:1111.0140v1*, **2011**.
(43) Scharfenberg, L.; Haak, H.; Meijer, G.; van de Meerakker, S. Y. T. *Phys. Rev. A* **2009**, *79*, 023410.
(44) Hänsel, W.; Reichel, J.; Hommelhoff, P.; Hänsch, T. W. *Phys. Rev. Lett.* **2001**, *86*, 608.
(45) Greiner, M.; Bloch, I.; Hänsch, T. W.; Esslinger, T. *Phys. Rev. A* **2001**, *63*, 031401.
(46) Trimeche, A.; Bera, M.; Cromières, J.-P.; Robert, J.; Vanhaecke, N. *Eur. Phys. J. D* **2011**, *65*, 263.
(47) Price, G. N.; Bannerman, S. T.; Viering, K.; Narevicius, E.; Raizen, M. G. *Phys. Rev. Lett.* **2008**, *100*, 093004.
(48) Bannerman, S. T.; Price, G. N.; Viering, K.; Raizen, M. G. *New J. Phys.* **2009**, *11*, 063044.
(49) Narevicius, E.; Bannerman, S. T.; Raizen, M. G. *New J. Phys.* **2009**, *11*, 055046.